Langmuir

Article

pubs.acs.org/Langmuir

Morphology Transformation of Hybrid Micelles Self-Assembled from Rod−Coil Block Copolymer and Nanoparticles

Chunhua Cai, Liquan Wang, Jiaping Lin,* and Xu Zhang

Shanghai Key Laboratory of Advanced Polymeric Materials, State Key Laboratory of Bioreactor Engineering, Key Laboratory for Ultrafine Materials of Ministry of Education, School of Materials Science and Engineering, East China University of Science and Technology, Shanghai 200237, China

Supporting Information

ABSTRACT: Hybrid polymeric micelles self-assembled from a mixture containing poly(γ-benzyl-L-glutamate)-*block*-poly(ethylene glycol) (PBLG-*b*-PEG) block copolymer and gold nanoparticles (AuNPs) were prepared. The effect of AuNPs on the self-assembly behavior of PBLG-*b*-PEG was studied both experimentally by transmission electron microscopy, scanning electron microscopy, and laser light scattering and computationally using dissipative particle dynamics (DPD) simulations. It was found that, the pure PBLG-*b*-PEG block copolymer self-assembles into long cylindrical micelles. By introducing AuNPs to the stock block copolymer solution, the formed aggregate morphology transforms to spherical micelles. The DPD simulation results well reproduced the morphological transformations observed in the experiments. And the simulation revealed that the main reason for the aggregate morphology transformation is the breakage of ordered packing of PBLG rods in micelle core by the added nanoparticles. Moreover, from the DPD simulations, the distribution information on nanoparticles was obtained. The nanoparticles were found to prefer to locate near the core/shell interface as well as in the core center of the micelles. The combination of experimental and simulation methods lead to a comprehensive understanding of such a complex self-assembly system.

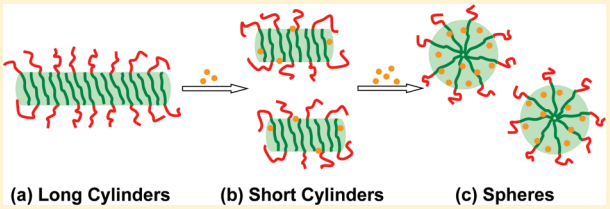

INTRODUCTION

Amphiphilic block copolymers are able to self-assemble into a variety of aggregates in dilute solution, such as micelles with a hydrophobic core surrounded by a hydrophilic shell.[1,2] The core−shell structure of the micelles provides a confined space for incorporation of various objects, such as drugs and genes.[3−6] Recently, polymeric micelles have been used as a template for controlling the organization of nanoparticles.[7−10] The micelles can significantly enhance the stability of dispersed state of nanoparticles in solution, which may facilitate their applications in catalysis, semiconductor, photonic, and biomimetic materials.[11−14]

To prepare block copolymer/nanoparticles hybrid micelles, both the chemical and physical strategies can be employed. In the chemical strategy, metal salts are first dispersed in solution and chemically combined with a specific ligand from polymers. Then through in situ metallization process, hybrid micelles were produced and the nanoparticles were chemically linked to the polymers by specific ligand.[15−21] In the physical strategy, presynthesized nanoparticles were physically embodied in the micelle core through comicellization.[22−24] Taton and co-workers have prepared core/shell nanoparticles via such an approach.[25−29] For example, in a study, polystyrene-*block*-poly(acrylic acid) (PS-*b*-PAA) block copolymer and 1-dodecanthiol-protected gold nanoparticles were first dissolved in dimethylformamide (DMF); then upon the addition of water, hybrid micelles with a gold core were produced.[24] Evidently, the physically encapsulation of nanoparticles is an easy manipulating method in preparing copolymer/nanoparticles hybrid micelles.

The physically introduced nanoparticles were found to have an effect on the parent micelle structure. Recently, Park et al. reported a self-assembly behavior of magnetic nanoparticles and PS-*b*-PAA block copolymers.[30] They revealed that the incorporation of nanoparticles drastically affects the assembly structure. For micelle-forming copolymers, the nanoparticles increase the effective volume taken up by PS, and hybrid vesicles were formed. For vesicle-forming copolymers, due to the solubilization of nanoparticles in PS domains, hybrid micelles were obtained. In addition to the experimental observations, advances in computation power and algorithm have opened up opportunities to investigate the self-assembly of block copolymer/nanoparticle mixture in solution. Various computer simulation approaches have been developed in the past years, for example, dissipative particle dynamics (DPD) simulations and self-consistent field theory (SCFT).[31−41] Results from computer simulations combined with experimental observations may provide comprehensive insight into the underlying principle governing the self-assembly of the block copolymer/nanoparticles in solution. Our group has used SCFT to study the effect of nanoparticles on the self-assembly behavior of coil−coil block copolymers.[42] It was shown that the

Received: December 15, 2011
Revised: January 31, 2012
Published: February 2, 2012

   dx.doi.org/10.1021/la204941w | Langmuir 2012, 28, 4515−4524

aggregate morphology changes from vesicles to a mixture of spheres and cylinders by increasing the particle radius and particle volume fraction. The predictions are well in agreement with the existing experiments.[42−44] However, the understanding of the influence of introduced nanoparticles on the self-assembly of block copolymers is still not deep enough.

As compared with coil−coil block copolymers, rod−coil block copolymers exhibit distinct self-assembly behaviors because the rod blocks prefer to take ordered packing mode in the self-assembly process.[45−48] Thus, it is expected that the change of the local ordered packing of rod blocks should greatly influence the self-assembly behavior of the rod−coil copolymers. As a matter of fact, in the homopolymer liquid crystal systems, it was found that the ordered packing of rigid polymer chains can be destroyed by introducing small portion of nanoparticles.[49] However, as far as we know, there is no work concerning the effect of nanoparticles on the self-assembly behavior of rod−coil block copolymers in solution.

On the other hand, increasing attention has been given to the self-assembly behavior of polypeptide-based copolymers.[50−54] Understanding their supramolecular assembly behaviors could be helpful for knowing the complex aggregation behaviors of polypeptides in organisms. In addition, polypeptides usually adopt a rigid α-helix conformation and can be used as an ideal model of rigid polymer segments. Researches on the self-assembly behavior of mixture systems comprising polypeptide-based rod−coil block copolymers and nanoparticles can not only deepen the understanding of the self-assembly behavior of rod−coil copolymers but also help the investigation of complex protein systems.

Herein, we investigated the self-assembly behavior of amphiphilic poly(γ-benzyl-L-glutamate)-*block*-poly(ethylene glycol) (PBLG-*b*-PEG) rod−coil block copolymer/gold nanoparticles (AuNPs) mixture system by both experimental and dissipative particle dynamics (DPD) simulation methods. The physically introduced nanoparticles were found to have significant effect on the self-assembly behavior of rod−coil block copolymers. Pure block copolymers self-assemble into long cylindrical micelles. With the introduction of AuNPs, spherical micelles were obtained. Simulations on the mixture system also indicated that, by increasing the concentration of nanoparticles, the aggregate structure transforms from cylinder to sphere. In addition to the morphological transformation, from the DPD simulation results, the location of nanoparticles and the order parameter of the copolymer chains were also obtained. On the basis of the experimental and DPD results, the mechanism of the morphological transformation of the block copolymer micelles as the function of added nanoparticles is suggested.

EXPERIMENTAL SECTION

Materials. Methoxypoly(ethylene glycol) amine (mPEG-NH_2, M_w = 20 000) was purchased from Sigma-Aldrich Inc. and dissolved in toluene in a flame-dried reaction bottle, followed by removing the toluene in high vacuum to obtain the sample used for copolymer synthesis. Hydrogen tetrachloroaurate ($HAuCl_4{\cdot}4H_2O$) (99.9%) was purchased from Shanghai Yiyang Chemical Inc. Dialysis bag (Membracel, 3500 molecular weight cutoff) was provided by Serva Electrophoresis GmbH. Tetrahydrofuran (THF), hexane, and 1,4-dioxane were all analytical grade, refluxed with sodium, and distilled immediately before use. All the other regents are of analytical grade and used without further purification.

Synthesis of PBLG-*b*-PEG Block Copolymer. PBLG-*b*-PEG block copolymer was synthesized by ring-opening polymerization of γ-benzyl-L-glutamate-*N*-carboxyanhydride (BLG-NCA) initiated by the terminal amino group of mPEG-NH_2.[48,55,56] The reactions was performed in a flame-dried reaction bottle under a dry nitrogen atmosphere at room temperature. After 3 days, the reaction mixture was poured into a large volume of anhydrous ethanol to precipitate the PBLG-*b*-PEG block copolymer. The precipitated product was dried under vacuum and then purified twice by repeated precipitation from a chloroform solution into a large volume of anhydrous methanol. Finally, the product was dried under vacuum and white power was collected.

Synthesis of Gold Nanoparticles. Monolayer-protected gold nanoparticles (AuNPs) were synthesized by the one-phase method according to the literature.[57−59] $HAuCl_4{\cdot}4H_2O$ and 1-dodecanethiol were dissolved in THF with concentrations of 0.02 and 0.2 mM, respectively. $NaBH_4$ was dissolved in deionized water with a concentration of 1 mM. 10 mL of 1-dodecanethiol THF solution was added under vigorous stirring to 50 mL of $HAuCl_4$ solution and stirred for ca. 10 min at room temperature, before 10 mL of $NaBH_4$ was added over a period of ca. 5 s. The color of the solution changed immediately from pale yellow to black upon the reductant addition. The reaction mixture was allowed to be stirred for 2 h. Purification of nanoparticles was performed using centrifugation and dialysis against water. The aqueous dispersion was freeze-dried, and AuNPs powder was obtained.

Preparation of Hybrid Micelles from Block Copolymer and AuNPs. To prepare the micelle solutions, the obtained PBLG-*b*-PEG and AuNPs were first dissolved in $CHCl_3$.[48] The initial concentration of polymer solution was 0.25 g/L, and the initial concentration of AuNPs was varied from 2.5×10^{-5} to 2.5×10^{-2} g/L. In the following step, the polymer and AuNPs solutions were mixed with equal volume to obtain stock solutions with various polymer/AuNPs weight ratios. Then ethanol, a selective solvent for PEG, was added at a rate of 1 drop every 3−4 s with vigorous stirring. A blue tint appearance of the solution indicates the formation of the aggregates. It should be noted that, in the present work, the term "aggregate" refers to the self-assembled micelles from block copolymer or block copolymer/nanoparticles mixture. In all the cases, for the final solution, the volume fraction of the ethanol was 0.6, and the polymer concentration became 0.05 g/L. Before the measurements, the obtained hybrid micelle solutions were stabilized at 20 °C for at least 3 days. The samples for LLS measurements were kept in the optical light scattering cell and sealed before the stabilization.

^{1}H NMR. The composition of the PBLG-*b*-PEG block copolymer was determined by the ^{1}H NMR spectrum (Avance 550, Bruker) with deuterated chloroform ($CDCl_3$) as solvent and tetramethylsilane (TMS) as an internal standard.

Gel Permeation Chromatography (GPC). The polydispersity index (PDI) of PBLG-*b*-PEG block copolymer was determined by GPC (Varian, PL GPC-50 plus) with DMF as mobile phase and narrow polydispersity PS as standard. The test was performed at 49 °C.

UV−vis Spectrum. UV−vis spectrum was obtained using a Shimadzu UV-2102PCS UV−vis scanning spectrophotometer at room temperature. AuNPs dispersion (in $CHCl_3$) was introduced in a quartz cell with 1 cm optical path length. Wavelengths between 200 and 800 nm were analyzed.

Fourier Transform Infrared Spectrum (FTIR). FTIR spectra of the samples were recorded on a Nicolet 5700 FTIR spectrometer at frequencies ranging from 400 to 4000 cm^{-1}. The solid AuNPs were thoroughly mixed with KBr and pressed into pellet form. For liquid 1-dodecanethiol, sample was prepared by casting a single drop of solution onto the KBr crystal. The tests were performed at room temperature.

Transmission Electron Microscopy (TEM). The morphologies of the AuNPs and self-assembled aggregates were examined by TEM (JEOL/JEM-2000EXII) operated at an accelerating voltage of 60 kV. Drops of AuNPs and micelle solutions were placed on a copper grid coated with carbon film and then were dried at room temperature. Before the observations, the micelle samples were stained by phosphotungstic acid ethanol solution (0.5 wt %).

Scanning Electron Microscopy (SEM). The surface profile of the aggregates was obtained from SEM (JSM-6460, JEOL) operated at an

accelerating voltage of 15 kV. The samples were prepared by placing drops of solution on a copper grid coated with carbon film and then were dried at room temperature. Before the observations, the samples were sputtered by carbon.

Laser Light Scattering Measurements (LLS). The structure of the aggregates was characterized by combining dynamic (DLS) and static light scattering (SLS) measurements, which were performed on a commercial LLS spectrometer (ALV/CGS-5022) equipped with an ALV-High QE APD detector and an ALV-5000 digital correlator using a He−Ne laser (the wavelength λ = 632.8 nm) as light source. All the measurements were carried out at 20 °C. From DLS testing, hydrodynamic radius (R_h) can be obtained, which indicates the radius of a hard sphere with the same translational diffusion coefficient and the same condition. While the SLS measurements gives the radius of gyration (R_g), which reflects the density distribution of the chain in real physical space. The details of the LLS testing method are provided in the Supporting Information.

SIMULATION METHOD AND MODEL

DPD Method. The dissipative particle dynamics (DPD), proposed by Hoogerbrugge and Koelman in 1992, is a simulation method of accessing larger length and time scale than molecular dynamics.[36,37] It has been developed for studying the phase behavior of soft matter systems such block copolymers in dilute solution.[38−41]

In DPD method, a bead represents the center of mass of an atomic cluster. The force acting on each bead includes conservative force, dissipative force, and random force. Therefore, the total force acted on a bead α is a sum of these three parts, which is given by

$$\mathbf{F}_\alpha = \sum_{\alpha\neq\beta} (\mathbf{F}^C_{\alpha\beta} + \mathbf{F}^D_{\alpha\beta} + \mathbf{F}^R_{\alpha\beta}) \quad (1)$$

The conservative force is the soft repulsion acting along the intermolecular vector, which is given by

$$\mathbf{F}^C_{\alpha\beta} = a_{\alpha\beta}\omega(r_{\alpha\beta})\hat{\mathbf{r}}_{\alpha\beta} \quad (2)$$

where $a_{\alpha\beta}$ is a maximum repulsion between bead α and β, and $r_{\alpha\beta} = |\mathbf{r}_\alpha - \mathbf{r}_\beta|$, $\hat{\mathbf{r}}_{\alpha\beta} = (\mathbf{r}_\alpha - \mathbf{r}_\beta)/r_{\alpha\beta}$. The weight function $\omega(r_{\alpha\beta})$ adopts the following form

$$\omega(r_{\alpha\beta}) = \begin{cases} 1 - r_{\alpha\beta}/r_c & r_{\alpha\beta} < r_c \\ 0 & r_{\alpha\beta} \geq r_c \end{cases} \quad (3)$$

Here, r_c is the cutoff radius, which was set to be 1.0.

The dissipative force is a hydrodynamic drag force and is given by

$$\mathbf{F}^D_{\alpha\beta} = -\gamma\omega^2(r_{\alpha\beta})(\hat{\mathbf{r}}_{\alpha\beta}\cdot\upsilon_{\alpha\beta})\hat{\mathbf{r}}_{\alpha\beta} \quad (4)$$

where $\boldsymbol{\upsilon}_{\alpha\beta} = \boldsymbol{\upsilon}_\alpha - \boldsymbol{\upsilon}_\beta$.

The random force corresponds to the thermal noise, which is represented as

$$\mathbf{F}^R_{\alpha\beta} = \sigma\omega(r_{\alpha\beta})\theta_{\alpha\beta}\hat{\mathbf{r}}_{\alpha\beta} \quad (5)$$

Here, $\theta_{\alpha\beta}$ is a random fluctuating variable with Gaussian statistics, which satisfies

$$\langle\theta_{\alpha\beta}(t)\rangle = 0 \quad (6)$$

$$\langle\theta_{\alpha\beta}(t)\theta_{\kappa\lambda}(t')\rangle = (\delta_{\alpha\kappa}\delta_{\beta\lambda} + \delta_{\alpha\lambda}\delta_{\beta\kappa})\delta(t - t') \quad (7)$$

The friction coefficient γ and the noise amplitude σ are related as $\sigma^2 = 2\gamma k_B T$, where T is the absolute temperature and k_B is the Boltzmann constant. In the present simulation ($k_B T$ = 1), we set γ = 4.5 and σ = 3.

Model. The rod blocks of rod−coil block copolymers are modeled as N_R beads of species **R** linked rigidly in a linear geometry, as shown in Figure 1. The distance between neighbor beads was fixed as 0.80. The coil blocks of rod−coil block copolymers are modeled as a linear bead−spring chain with N_C beads of species **C** bonded together via a harmonic potential. The harmonic spring force is given by $\mathbf{F}^S_{\alpha\beta} = k(1 - r_{\alpha\beta}/r_{eq})\hat{\mathbf{r}}_{\alpha\beta}$. The spring constant k was chosen to be 100, and the equilibrium bond distance r_{eq} was set as 0.80. The different choices of k and r_{eq} distance should bring in no apparent discrepancies from the static or dynamic properties of polymers, except for altering the average bond length.[60,61] Therefore, the choice of these two parameters in this work is not specific, except for satisfying following two conditions: (1) keep the coil blocks significantly flexible, and therefore a smaller value of k = 100 was chosen; (2) keep the equilibrium bond distance equal to the distance between neighbor beads in the rod blocks (for the simplicity of setting the bead numbers, which will be discussed below), and also keep this distance in the range of cutoff radius (r_{eq} (= 0.8) < r_c (= 1.0)). This choice is only a coarse-grained selection to show the constraint imposed upon connected beads of a polymeric chain.

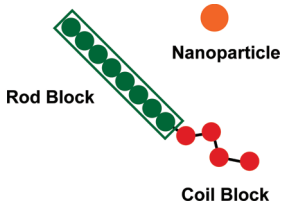

Figure 1. DPD model of the R10C4 rod−coil block copolymer and the nanoparticle.

The remainder task is to determine the N_R and N_C from the experiments. There are several coarse-grained mapping method to link the simulations with the experiments. For example, the models can be chosen such that the bulk density of pure species[62] or the relative lengths of the blocks[48] matches experimental data. In this study, the model was chosen by renormalizing both the bulk weight densities and block lengths. In the simulation, the mass of beads (m = 1) and bead distance/equilibrium bond length (0.8) for different beads are fixed. From the experiments, we learned that the molecular weights of rod blocks and coil blocks are 138 000 and 20 000, respectively. First, the number of DPD beads was renormalized by keeping the bulk density identical in the simulations and experiments, and then a ratio of 138 000/20 000 was obtained. In this case, 3.6 DPD beads for the PBLG form a 0.54 nm helix (or modeling rod),[48] while 1 DPD bead for the PEG occupies 0.35 nm.[48,63] Second, the number of DPD beads was renormalized by the length of rod block and coil blocks (the bead distance is equal to the equilibrium bond length), and we obtained the relative number of DPD beads for rod and coil blocks as (138 000 × 0.54/3.6):(20 000 × 0.35/1) ≈ 10:3.4. As a result, the model of R10C4 rod−coil block copolymers composed of 10 rod **R** beads and 4 coil **C** beads was adopted in the study.

In addition, the nanoparticles and cluster of solvents are modeled as a single bead. Hence, the system contains two types of single beads, where one is nanoparticles and the other is solvent clusters. In the simulations, the weight concentration of

dx.doi.org/10.1021/la204941w | Langmuir 2012, 28, 4515−4524

block copolymers is fixed as 10 wt %. The polymer concentration in the simulation is higher than that in the experiments. The reason that we do not choose a lower concentration in the simulation is due to the limitation of computer simulations. The polymer concentration should have an effect on the formation of aggregates. However, since the simulations started from the fact that the pure rod−coil block copolymers form cylindrical micelles in the solution and investigated the effect of the nanoparticle concentration on the morphology of cylindrical micelles, the effect of polymer concentration should be less marked. Overall, building such a model is not intended to represent a specific chemistry of the PBLG-*b*-PEG/AuNPs solution but is intended to capture the characteristics of the morphological transformations. In the models, the **R**, **C**, **P**, and **S** denote the rod PBLG blocks, coil PEG blocks, AuNPs, and solvents, respectively.

The simulations were performed in the 30 × 30 × 30 three-dimensional space with periodic boundary conditions. The NVT ensemble was adopted in the simulations. The units of mass, length, time, and energy are defined by m, r_c, τ, and k_BT, respectively. The time unit τ can be obtained by $\tau = (mr_c^2/k_BT)^{1/2}$, and its real value can be estimated by matching the simulated lateral diffusion coefficient to the experimental measured value. The Newton equations for all bead positions and velocities are integrated by a modified version of the velocity-Verlet algorithm with step size $\Delta t = 0.04\tau$. The modified version of the velocity-Verlet algorithm is given as[39]

$$\mathbf{r}_\alpha(t + \Delta t) = \mathbf{r}_\alpha(t) + \Delta t\mathbf{v}_\alpha(t) + 0.5(\Delta t)^2\mathbf{F}_\alpha(t) \quad (8)$$

$$\tilde{\mathbf{v}}_\alpha(t + \Delta t) = \mathbf{v}_\alpha(t) + 0.5\Delta t\mathbf{F}_\alpha(t) \quad (9)$$

$$\mathbf{F}_\alpha(t + \Delta t) = \mathbf{F}_\alpha(\mathbf{r}(t + \Delta t), \tilde{\mathbf{v}}(t + \Delta t)) \quad (10)$$

$$\mathbf{v}_\alpha(t + \Delta t) = \mathbf{v}_\alpha(t) + 0.5\Delta t(\mathbf{F}_\alpha(t) + \mathbf{F}_\alpha(t + \Delta t)) \quad (11)$$

The density of the system was chosen to be $\rho = 3$, and hence the total number of DPD beads is 81 000. The interaction strengths between DPD beads with same species are completely compatible, which is determined as $a_{\alpha\alpha} = 75k_BT/\rho = 25$. For PBLG−PEG block copolymers, the PBLG is hydrophobic and the PEG is hydrophilic, and therefore the a_{RS} and a_{CS} are set to be 120 and 25, respectively. In addition, the PBLG is incompatible with PEG and $a_{RC} = 80$ was set. The a_{RC} is smaller than a_{RS}, implying PBLG is more compatible with PEG than solvents. The nanoparticles are hydrophobic and more compatible with rod PBLG than PEG. Therefore, we set the repulsive parameter a_{PS} to be 80, and a_{PR} (= 25) < a_{PC} (= 60).

Order Parameter. A quantitative measure for the degree of packing of rod blocks is the order parameter S. The order parameter S_i for the ith rod block can be defined by as follows

$$S_i = \frac{3(\mathbf{u}_i\cdot\mathbf{u}_d)^2 - 1}{2} \quad (12)$$

where $\mathbf{u}_i$ is normalized vector of the ith rod block and $\mathbf{u}_d$ is the normalized vector of orientation direction. By choosing different $\mathbf{u}_d$, we can obtain various S, where the S of rod blocks within the core is calculated as the average value of S_i. The order parameter for rod block is determined as the maximum value of S by taking into account the up−down symmetry of the rod block. The angle θ between ith block and normalized vector of orientation direction is given by

$$\cos(\theta) = \mathbf{u}_i\cdot\mathbf{u}_d \quad (13)$$

RESULTS AND DISCUSSION

Characterization of PBLG-*b*-PEG Block Copolymer. PBLG-*b*-PEG block copolymer was synthesized via a standard NCA procedure, with terminal amino group of mPEG-NH_2 as initiator. After purification, PBLG-*b*-PEG block copolymer with narrow polydispersity was obtained. As shown in Figure 2a,

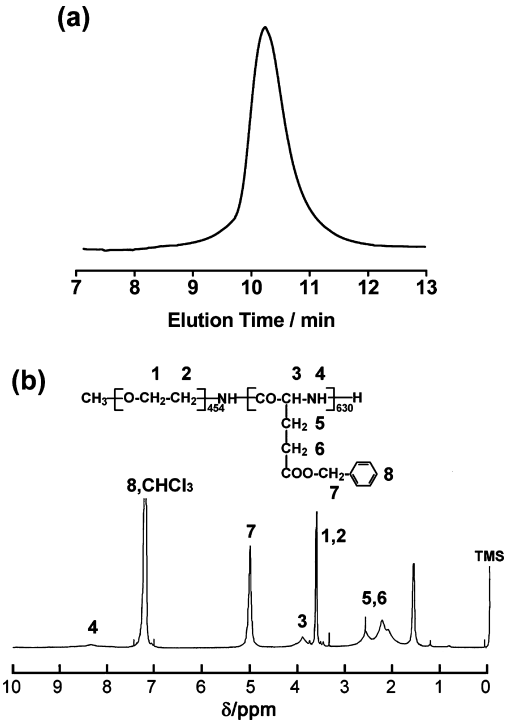

Figure 2. (a) GPC trace of the PBLG-*b*-PEG block copolymer with DMF as eluent solvent and narrow polydispersity polystyrene as standards. (b) ^{1}H NMR spectrum of PBLG-*b*-PEG block copolymer in $CDCl_3$.

GPC analysis in DMF reveals a unimodal and symmetric peak, which indicates a well-controlled polymerization process. Since the GPC testing was performed with narrow polydispersity polystyrene as standards, the obtained molecular weight is depart from the real value; thus, only the polydispersity index was adopted. From the GPC testing, the polydispersity index of the block copolymer was determined to be a narrow value of 1.17.

The molecular weight of the block copolymer was calculated from the ^{1}H NMR spectrum. Figure 2b shows the ^{1}H NMR spectrum of PBLG-*b*-PEG block copolymer in $CDCl_3$. It can be clearly seen that all signals characteristic of PEG and PBLG blocks are visible. The signal at δ = 3.6 ppm is ascribed to methyl protons (1, 2) of the PEG block; the resonance signals of protons on amide group (4), phenyl group (8), methylene group of benzyl (7), methenyl group (3), and methylene groups (5, 6) of PBLG block occur at δ = 8.4, 7.3, 5.1, 3.9, and 1.8−2.7 ppm, respectively. Since the degree of polymerization (DP) of the PEG block is known (454), the molecular weight of PBLG block can be calculated by the peak intensities of the methylene proton signal (5.1 ppm) of polypeptide and the

dx.doi.org/10.1021/la204941w | *Langmuir* 2012, 28, 4515−4524

methylene proton signal (3.6 ppm) of PEG.[48,64] According to the NMR analysis, the DP of PBLG block is calculated to be 630; thus, the molecular weight of PBLG block is 138 000. In addition, we have also synthesized PBLG-*b*-PEG block copolymers with various block length of PBLG and PEG, for example, $PBLG_{30000}$-*b*-PEG_{20000} and $PBLG_{73000}$-*b*-PEG_{5000}; the subscripts denote the molecular weight for each segment.

Characterization of Gold Nanoparticles. The gold nanoparticles (AuNPs) were synthesized through a simple one-phase method. The obtained nanoparticles are covered with a monolayer of 1-dodecanethiol and can disperse in organic solvent, e.g., $CHCl_3$. Figure 3 presents the DLS result of the monolayer protected gold nanoparticles in $CHCl_3$. The mean diameter of the AuNPs is determined to be ca. 11 nm. The TEM image reveals these AuNPs are spherical in shape, and the size of nanoparticles has some dispersity (see inset of Figure 3). As compared with DLS testing, TEM observation gives a smaller diameter of nanoparticle. The reason is that the size of the AuNPs determined by the DLS testing includes the length of tethered alkyl chains, while TEM observation is operated under dry state and reflects the solid region of the nanoparticles.

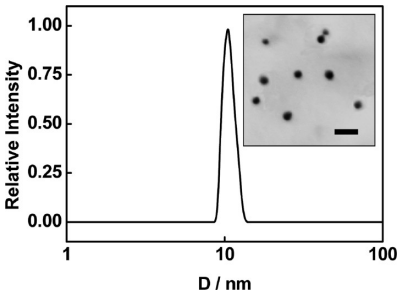

Figure 3. Diameter distribution of monolayer-protected AuNPs dispersed in $CHCl_3$ tested by DLS at scattering angle of 90°. The inset shows the TEM image of AuNPs dispersed in $CHCl_3$. Scale bar represents 25 nm.

AuNPs are known to exhibit a surface plasmon resonance (SPR) in the visible region due to their nanoscaled size. Figure 4 shows the UV−vis spectrum of the monolayer-protected AuNPs in $CHCl_3$. The surface plasmon absorption at ca. 515 nm is observed, which is in agreement with the average size of the nanoparticles.[65,66] The inset in Figure 4 shows the FTIR spectra of 1-dodecanethiol (curve a) and monolayer protected AuNPs (curve b). In the curve a, the S−H stretching band at 2552 cm^{-1} was detected.[67] However, for the monolayer-protected AuNPs, the S−H stretching band absorption disappeared, indicating the strong interaction between −SH group and Au atoms.

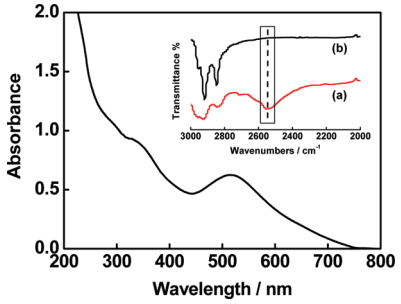

Figure 4. UV−vis spectrum of monolayer-protected AuNPs dispersed in $CHCl_3$. The inset shows the FTIR spectra of (a) 1-dodecanethiol and (b) monolayer-protected AuNPs. The broken line indicates the position of the S−H stretching band (2552 cm^{-1}).

Aggregate Morphologies Observed by TEM and SEM. Figure 5 shows the aggregate morphologies of the hybrid micelles formed by PBLG-*b*-PEG block copolymer with various amount of AuNPs in $CHCl_3$/ethanol mixed solution. As shown in Figure 5a, pure block copolymers form cylindrical micelles. The length of the cylinders is in the range of 150 nm−1 μm. The diameter of the cylinders is about 90 nm. The SEM image shown in Figure 5e clearly gives a three-dimensional shape of the cylinders. When the AuNPs is introduced, as shown in Figure 5b, short cylinders with length of about 150 nm were produced. These short cylinders have a same diameter with the long cylinders, which indicates that the short cylinders could be fragments of long cylinders. As the AuNPs mass percent (to block copolymer) increases to 1 wt %, the diameter of the aggregates increases, and ellipse-like structures were obtained (Figure 5c). Further increasing the AuNPs mass percent to 2−10 wt % leads to the formation of spherical micelles. Figure 5d shows the TEM image of the spherical hybrid micelles formed with 3 wt % AuNPs. From the magnified image in the inset in Figure 5d, AuNPs can be clearly seen in the micelle core. The regular spherical image of the hybrid micelles was observed from SEM testing, as shown in Figure 5f. When the mass percent of AuNPs is higher than 10 wt %, the micelles become unstable, and participates are produced. In the present work, since the concentration of the nanoparticles is very low and also the nanoparticles are protected by a monolayer of alkyl chains, the aggregation tendency of the nanoparticles is neglectable. The nanoparticles are in nonaggregated state, which can be evidenced by the TEM observations (see inset of Figure 5d).

As a control experiment, we studied self-assembly behavior of PBLG-*b*-PEG/AuNPs hybrid systems containing the block copolymers with various molecular weights. For copolymers with shorter PBLG chains ($PBLG_{30000}$-*b*-PEG_{20000}), they self-assembled into spherical micelles. When the AuNPs were incorporated, spherical micelles still formed, but the aggregate size slightly increased. For $PBLG_{73000}$-*b*-PEG_{5000} block copolymer, cylindrical micelles were obtained from pure copolymer. And a similar aggregate morphology transformation from cylinder to sphere was observed, as nanoparticles were introduced into the system. However, owing to the lower weight fraction of solvophilic PEG segments in the block copolymer, the hybrid micelles become unstable at relative lower AuNPs concentrations.

Aggregate Size and Structure Studied by LLS. The aggregate morphology transformation as a function of nanoparticle concentration was further studied by DLS and SLS. As shown in Figure 6, both the average hydrodynamic radius ($\langle R_h \rangle$) and the average radius of gyration ($\langle R_g \rangle$) decrease markedly with increasing AuNPs mass percent from 0 to 3 wt % and then increases slightly with more AuNPs added. The $\langle R_g \rangle$ value decreases more sharply than $\langle R_h \rangle$ value does. The decrease of $\langle R_h \rangle$ and $\langle R_g \rangle$ values can be attributed to the morphology change from long cylindrical micelle to spherical micelle.[68] As the AuNPs concentration further increases, both $\langle R_h \rangle$ and $\langle R_g \rangle$ values level off, indicating that the effect of AuNPs becomes less pronounced. It should be noted that, for the nonspherical cylindrical micelles, the obtained $\langle R_h \rangle$ value is an apparent one, and thus it is smaller than its dimension observed from microscopies.

The aggregate structure change can also be viewed in terms of the ratio of $\langle R_g \rangle / \langle R_h \rangle$, which is sensitive to the particle

dx.doi.org/10.1021/la204941w | *Langmuir* 2012, 28, 4515−4524

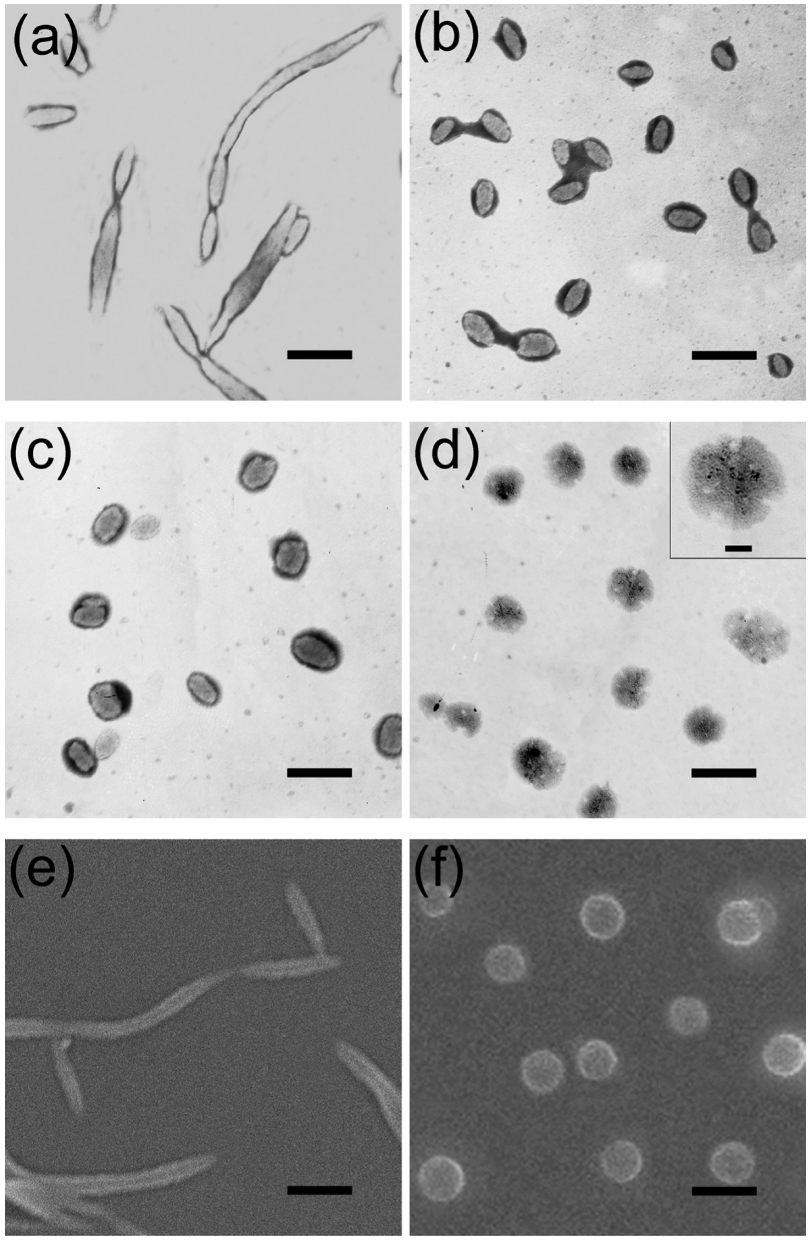

Figure 5. TEM images of PBLG-*b*-PEG/AuNPs hybrid micelles with various AuNPs mass percent: (a) 0, (b) 0.1, (c) 1, and (d) 3 wt %. The inset in (d) shows the AuNPs enclosed in hybrid micelle. SEM images of PBLG-*b*-PEG/AuNPs hybrid micelles with various AuNPs mass percent: (e) 0 and (f) 3 wt %. Scale bars represent 250 nm, and the scale bar in the inset in (d) represents 50 nm.

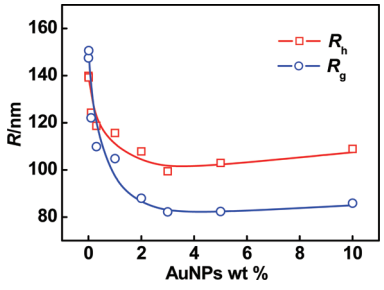

Figure 6. Plots of $\langle R_h \rangle$ and $\langle R_g \rangle$ versus AuNPs mass percent for the PBLG-*b*-PEG/AuNPs hybrid micelles.

shape.[69,70] It is well-known that $\langle R_g \rangle / \langle R_h \rangle$ decreases as the structure change from an extended manner to a sphere. As shown in Figure 7, $\langle R_g \rangle / \langle R_h \rangle$ continuously decreases from 1.1 to 0.8, when the aggregate morphology transforms from extended cylinder to spherical micelle with increasing AuNPs concentration in the range between 0 and 3 wt %. Further increasing AuNPs concentration influences little on the $\langle R_g \rangle / \langle R_h \rangle$ value. Such DLS and SLS results are in reasonable agreement with TEM and SEM observations for the aggregate morphology transformations.

Dissipative Particle Dynamics Simulations. As revealed by the experimental results, the introduction of AuNPs exhibits a pronounced effect on the aggregate morphology. However, detailed information such as chain packing and nanoparticle location is difficult to be obtained directly from the experiments. In order to gain a comprehensive understanding of the morphological transformations, we further carried out a DPD simulation in this work. A model consisting of rod−coil block copolymer and single bead was constructed to correspond to

dx.doi.org/10.1021/la204941w | *Langmuir* 2012, 28, 4515−4524

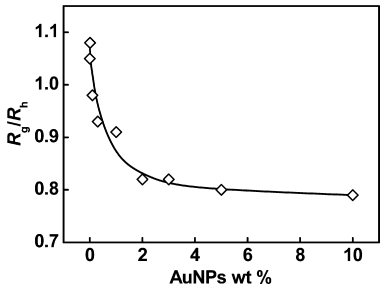

Figure 7. Plots of $\langle R_g \rangle / \langle R_h \rangle$ versus AuNPs mass percent for the PBLG-*b*-PEG/AuNPs hybrid micelles.

PBLG-*b*-PEG block copolymer and AuNPs, respectively. The simulations provide more information for the insight into the self-assembly process, such as the distributions of block copolymers and nanoparticles in micelle and the order parameters of rod blocks.

The self-assembly of pure R10C4 block copolymers in dilute solution was first studied. As shown in Figure 8a, the block copolymers self-assemble into a cylindrical micelle. The rod blocks (green) are regularly packed into the core, whereas the coil blocks (red) cover the cores to form shell. From the simulations, the packing mode of the rod blocks was also observed. Within the core, the rod blocks are interdigitated and their long axes are aligned orientationally. The orientation vector is gradually changed along the long-center axis of the cylinder and forms a twisted structure. To further gain the information about the orientation of rod blocks, the vector product $\cos(\theta)$ between rod blocks and long axis was calculated. As shown in Figure 8b, the value of $\cos(\theta)$ is about 0.924 or −0.924, and it is independent of the position along the cylinder. The opposite values reflect that the block copolymers are packed both in parallel and antiparallel fashion with each other. From the value of $\cos(\theta)$, the angle between the rod blocks and long-center axis of cylinder is calculated to be 22.5°.

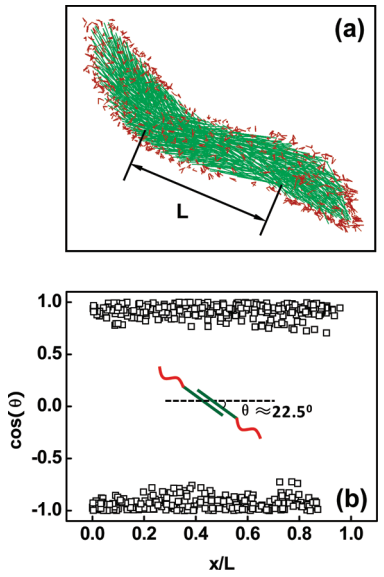

Figure 8. (a) Cylindrical micelle self-assembled from R10C4 rod−coil block copolymers in dilute solution. The green and red lines are assigned to rod and coil blocks, respectively. (b) Vector product $\cos(\theta)$ between rod blocks and long axis as a function of the position along the long axis. The inset shows a sketch of the rod alignment with long axis.

It is noted that the arrangement of rod blocks in the cylindrical micelle matches the essential characteristic of the chiral liquid crystal structures. In the assembly systems, this structure is rarely revealed, and the chiral liquid crystal structure is an interesting finding of this study. In our previous work, by using Brownian dynamics (BD) simulations, we found that the rod−coil block copolymers self-assemble into aggregates with rod block orderly packed in the core. The packing of the rods exhibits chiral nematic fashion.[71] The difference between these two structures is the orientational angles between the rod block and the long-center axis. The orientational angle for our previous work is 90°, while for the present finding, it is about 22.5°. We can regard the core packing in our DPD simulation and BD simulation as chiral semetic C and chiral semetic A phases, respectively. The semetic C phase is found to be formed at strong interaction strengths between rod and coil blocks for rod−coil block copolymer melts.[72,73] Therefore, we think that the difference in repulsion strengths may be a reason for forming different core packing; i.e., the repulsion between rod and coil blocks in the BD calculations is smaller than that in DPD. In addition, the discrepancy may also be resulted from the other influence factors such as block lengths and simulation methods. Nevertheless, it seems a common law that the rod−coil block copolymers can self-assemble into the aggregates with chiral liquid crystal structures in the core.

The typical simulation predictions for the effect of nanoparticle (NP) on the self-assembly structure are presented in Figure 9. When the mass percent of nanoparticles is lower (0.62 wt %), the R10C4/NPs mixture still self-assembles into the cylindrical micelles (Figure 9a). As the mass percent of nanoparticles increases (1.48 wt %), the cylindrical micelles transfer into short cylinders, as shown in Figure 9b. At the higher concentration of nanoparticles, spherical micelles are formed. Figures 9c and 9d show the spherical structures formed with mass percent of nanoparticles of 1.85 and 2.47 wt %, respectively. This morphological transformation well reproduces the experimental observations for PBLG-*b*-PEG/AuNPs mixture in solution.

Figure 10 presents the density distributions of rod blocks, coil block, and nanoparticles in cylindrical and spherical micelles. For cylindrical micelles, we plotted the distributions in the front part of cylindrical micelles, along the arrow shown in the inset of Figure 10a. The rod blocks assume a single-peak distribution, and the coil blocks exhibit a double-peak distribution. This is the essential characteristic for cylindrical micelles. The distribution of nanoparticles is more complex, which is presented as a triple-peak distribution. This means that the nanoparticles prefer to distribute at the core/shell interface and in the center of interior core. For spherical micelles, as shown in Figure 10b, the nanoparticles and coil blocks exhibit similar distributions as in cylindrical micelles. However, the distribution of rod blocks is different, and it has double peaks. Such phenomena are resulted from the substantive incorporation of nanoparticles in the center of hydrophobic cores.

As stated above, for pure copolymer micelles, the rod blocks are found to take ordered packing mode (see Figure 8a,b). To evaluate the effect of nanoparticles on the packing mode of rod blocks, the order parameter of rod blocks in the various micelles was examined. Figure 11 shows the order parameter (S) of rod blocks as a function of the mass percent of nanoparticles. For pure copolymer micelle, the order parameter

dx.doi.org/10.1021/la204941w | *Langmuir* 2012, 28, 4515−4524

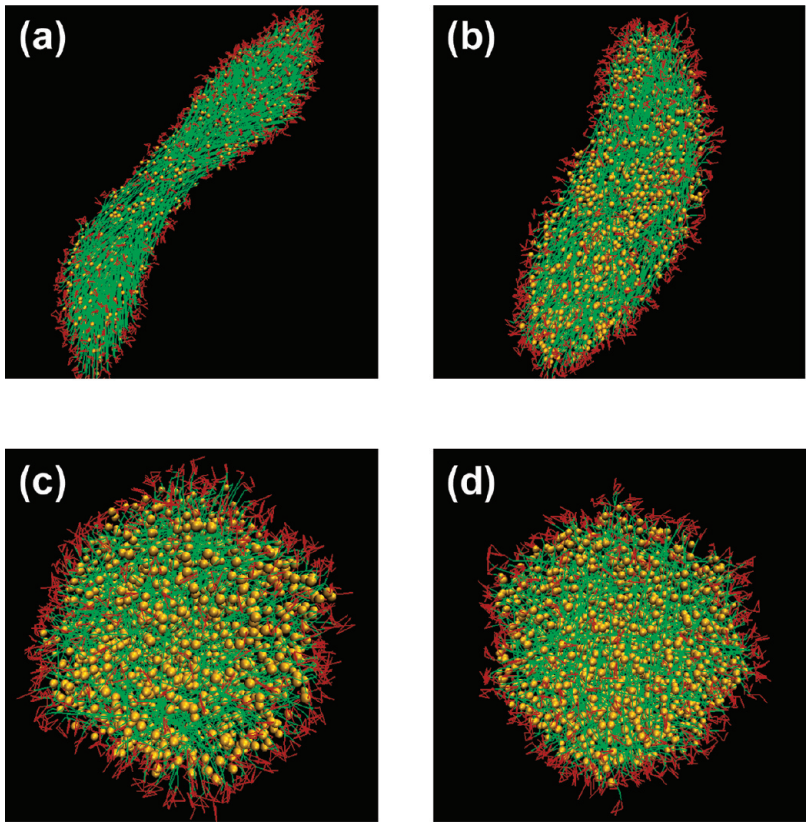

Figure 9. Micelles self-assembled from R10C4 rod−coil block copolymer/nanoparticles mixture in dilute solution. The mass percent of nanoparticles is (a) 0.62, (b) 1.48, (c) 1.85, and (d) 2.47 wt %. The green and red lines are assigned to rod and coil blocks, respectively, whereas the orange particles denote nanoparticles.

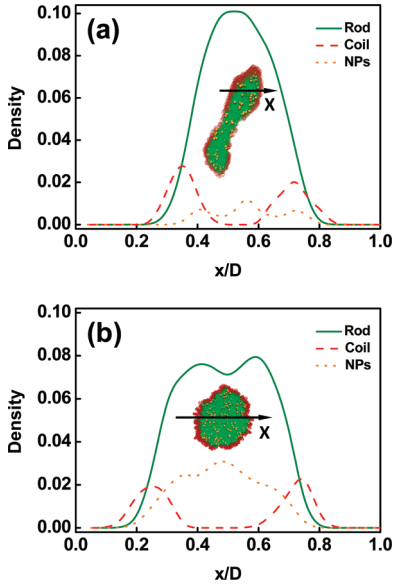

Figure 10. Density distribution of rod blocks, coil blocks, and nanoparticles on a cross section of the aggregates marked with an arrow in the inset for R10C4 rod−coil block copolymer/nanoparticles mixture at different nanoparticle mass percent: (a) 0.62 and (b) 2.47 wt %.

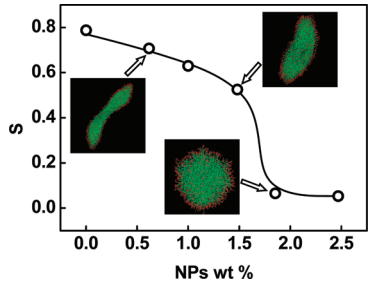

Figure 11. Order parameter S of rod blocks as a function of the concentration of nanoparticles. The insets show the corresponding structures of rod−coil block copolymers, and the nanoparticles are not shown for clarity.

is about 0.8, implying that the rod blocks are regularly orientated in core. With increasing the concentration of nanoparticles, the order parameter gradually decrease until the formation of spherical micelles. It was found that the order parameter of rod blocks in spherical micelles is dramatically reduced, and the value approaches zero. This indicates that the block copolymers are randomly packed in spherical micelle.

From the above experimental and simulation results, we learned that the introduction of AuNPs destroys the ordered packing of PBLG rods in micelle core and thus changes the aggregate morphology. It is well-known that in concentrated organic solutions PBLG homopolymers take side-by-side ordered packing mode and form liquid crystal structures.[74] For PBLG-based block copolymers, PBLG rods can also form liquid crystal domains.[75] In the present work, PBLG-*b*-PEG block copolymers self-assemble into cylindrical micelles in a selective solution (Figure 5a), in which PBLG rods are orderly packed into twist structure in the micelle core and the flexible PEG blocks are outspread to stabilize the aggregates (Figure 8). When the AuNPs are incorporated into micelle core, the

dx.doi.org/10.1021/la204941w | *Langmuir* 2012, 28, 4515−4524

distance between PBLG rods increases, which decreases the attraction between the PBLG rods; resultantly, the liquid crystal structure is gradually destroyed.[47] For systems containing lower volume fraction of nanoparticles, the ordered arrangement of PBLG rods in the micelle core was partially destroyed, and short cylinders were produced (Figures 5b and 9b). When the concentration of AuNPs increases, the sustaining filling of the nanoparticles destroys the global ordering of the PBLG rods. With the breakage of PBLG liquid crystal structure, spherical micelle is preferred (Figures 5d and 9d), which can lower the system energy.[76,77]

The nanoparticles were found to prefer to distribute at the core/shell interface and in the center of interior core (Figure 10a,b). However, the distribution details of the nanoparticles still have some changes with variation in the aggregate morphology. When the concentration of nanoparticles is lower, they can effectively be loaded in the core/shell interface of long cylinders (Figure 9a). Increasing the concentration of nanoparticles, short cylinders produced, which offered more open ends for localization of nanoparticles (Figures 9b and 10a). For the spherical micelles formed at higher concentration of nanoparticles, nanoparticle is substantive incorporated in the center of hydrophobic cores, which results in a double-peak distribution of PBLG rods (Figures 9c,d and 10b). In addition, the random distribution of PBLG rods in spherical micelles provides large interface spaces for filling nanoparticles.

Finally, we wish to emphasize the importance of the combination of experimental and computer simulation methods in investigating the self-assembly behavior of complex systems. From the experimental studies, direct but apparent results are ready to be observed. However, the mechanism behind the phenomena usually could be difficult to be obtained straightly. Simulation predictions based on model systems can not only reproduce the experimental observations but also provide additional information, such as chain distributions. Combining the experimental and simulation work is therefore an effective strategy for the investigation of complicated polymer self-assembly. In the present study, the aggregate morphologies of PBLG-*b*-PEG/AuNPs hybrid micelles were directly observed from TEM and SEM testing, and the aggregate sizes were monitored by LLS measurement. On the aiding of simulation predictions of density distributions of copolymers and nanoparticles, the inherent structure and mechanism of the formation of hybrid micelles were obtained, which deepens our understanding on the self-assembly process of such complex system.

CONCLUSIONS

In summary, we presented an example of influence of the nanoparticles on the self-assembly behavior of the rod−coil PBLG-*b*-PEG block copolymer in solution. Computer simulation was applied to deepen the understanding of the formation mechanisms of the hybrid micelles. For the pure block copolymers, long cylinders are formed. In the cylindrical micelle core, rod blocks were found to pack into a twisted structure. When the AuNPs were incorporated into the micelle core, the long cylindrical micelles transform into short cylinders and then to spherical micelles. The breakage of ordered packing of PBLG rods by the added AuNPs takes response for such an aggregate morphological transformation. Furthermore, the AuNPs were found to prefer to locate near the core/shell interface and in the core center of the aggregates. This study enriched our knowledge in the supramolecular chemistry of the self-assembly of block copolymer/nanoparticle systems and may provide useful guidance for designing hybrid polymeric composites with definite microstructures.

ASSOCIATED CONTENT

Supporting Information

Details of the LLS testing method. This material is available free of charge via the Internet at http://pubs.acs.org.

AUTHOR INFORMATION

Corresponding Author

*Tel: +86-21-64253370; Fax: +86-21-64251644; e-mail: jlin@ecust.edu.cn, jplinlab@online.sh.cn.

Notes

The authors declare no competing financial interest.

ACKNOWLEDGMENTS

This work was supported by National Natural Science Foundation of China (50925308), Program for Changjiang Scholars and Innovative Research Team in University (No. IRT0825), and National Basic Research Program of China (No. 2012CB933600). Support from projects of Shanghai municipality (10GG15, 08DZ2230500 and B502) is also appreciated.

REFERENCES

(1) Riess, G. *Prog. Polym. Sci.* **2003**, *28*, 1107.
(2) Bhargava, P.; Tu, Y.; Zheng, J. X.; Xiong, H.; Quirk, R. P.; Cheng, S. Z. D. *J. Am. Chem. Soc.* **2006**, *128*, 2745.
(3) Rosler, A.; Vandermeulen, G. W. M.; Klok, H. A. *Adv. Drug Delivery Rev.* **2001**, *53*, 95.
(4) Soppimath, K. S.; Liu, L.; Seow, W. Y.; Liu, S.; Powell, R.; Chan, P.; Yang, Y. *Adv. Funct. Mater.* **2007**, *17*, 355.
(5) Lin, J.; Zhu, J.; Chen, T.; Lin, S.; Cai, C.; Zhang, L.; Zhuang, Y.; Wang, X.-S. *Biomaterials* **2009**, *30*, 108.
(6) Wei, L.; Cai, C.; Lin, J.; Chen, T. *Biomaterials* **2009**, *30*, 2606.
(7) Love, J. C.; Estroff, L. A.; Kriebel, J. K.; Nuzzo, R. G.; Whitesides, G. M. *Chem. Rev.* **2005**, *105*, 1103.
(8) Daniel, M.-C.; Astruc, D. *Chem. Rev.* **2004**, *104*, 293.
(9) Forster, S.; Antonietti, M. *Adv. Mater.* **1998**, *10*, 195.
(10) Mai, Y.; Eisenberg, A. *J. Am. Chem. Soc.* **2010**, *132*, 10078.
(11) Balazs, A.; Emrick, T.; Russel, T. *Science* **2006**, *314*, 1107.
(12) Hamley, I. W. *Angew. Chem., Int. Ed.* **2003**, *42*, 1692.
(13) Shenhar, R.; Norsten, T.; Rotello, V. *Adv. Mater.* **2005**, *17*, 657.
(14) Comotti, M.; Li, W. C.; Spliethoff, B.; Schuth, F. *J. Am. Chem. Soc.* **2006**, *128*, 917.
(15) Luo, S.; Xu, J.; Zhang, Y.; Liu, S.; Wu, C. *J. Phys. Chem. B* **2005**, *109*, 22159.
(16) Nuopponen, M.; Tenhu, H. *Langmuir* **2007**, *23*, 5352.
(17) Hou, G.; Zhu, L.; Chen, D.; Jiang, M. *Macromolecules* **2007**, *40*, 2134.
(18) Radziuk, D.; Shchukin, D.; Skirtach, A.; Mohwald, H.; Sukhorukov, G. *Langmuir* **2007**, *23*, 4612.
(19) Koh, H.-D.; Kang, N.-G.; Lee, J.-S. *Langmuir* **2007**, *23*, 11425.
(20) Sidorov, S. N.; Bronstein, L. M.; Kabachii, Y. A.; Valetsky, P. M.; Soo, P. L.; Maysinger, D.; Eisenberg, A. *Langmuir* **2004**, *20*, 3543.
(21) Wang, Z.; Skirtach, A. G.; Xie, Y.; Liu, M.; Mohwald, H.; Gao, C. *Chem. Mater.* **2011**, *23*, 4741.
(22) Chen, H. Y.; Abraham, S.; Mendenhall, J.; Delamarre, S. C.; Smith, K.; Kim, I.; Batt, C. A. *ChemPhysChem* **2008**, *9*, 388.
(23) Lecommandouxa, S.; Sandreb, O.; Checota, F.; Rodriguez-Hernandeza, J.; Perzynski, R. *J. Magn. Magn. Mater.* **2006**, *300*, 71.
(24) Ruan, G.; Vieira, G.; Henighan, T.; Chen, A.; Thakur, D.; Sooryakumar, R.; Winter, J. O. *Nano Lett.* **2010**, *10*, 2220.
(25) Kang, Y.; Taton, T. *Angew. Chem., Int. Ed.* **2005**, *44*, 409.
(26) Kang, Y.; Taton, T. *Macromolecules* **2005**, *38*, 6115.
(27) Kim, B.; Taton, T. *Langmuir* **2007**, *23*, 2198.

(28) Kim, B.-S.; Qiu, J.-M.; Wang, J.-P.; Taton, T. A. *Nano Lett.* **2005**, *5*, 1987.
(29) Chen, Y.; Cho, J.; Young, A.; Taton, T. A. *Langmuir* **2007**, *23*, 7491.
(30) Hickey, R. J.; Haynes, A. S.; Kikkawa, J. M.; Park, S.-J. *J. Am. Chem. Soc.* **2011**, *133*, 1517.
(31) Zhuang, Y.; Lin, J.; Wang, L.; Zhang, L. *J. Phys. Chem. B* **2009**, *113*, 1906.
(32) He, X.; Liang, H.; Huang, L.; Pan, C. *J. Phys. Chem. B* **2004**, *108*, 1731.
(33) Wang, R.; Tang, P.; Qiu, F.; Yang, Y. *J. Phys. Chem. B* **2005**, *109*, 17120.
(34) Matson, M. W.; Schick, M. *Phys. Rev. Lett.* **1994**, *72*, 2660.
(35) Drolet, F.; Fredrickson, G. H. *Macromolecules* **2001**, *34*, 5317.
(36) Koelman, J. M. V. A.; Hoogerbrugge, P. J. *Europhys. Lett.* **1993**, *21*, 363.
(37) Hoogerbrugge, P. J.; Koelman, J. M. V. A. *Europhys. Lett.* **1992**, *19*, 155.
(38) Groot, R. D.; Madden, T. J.; Tildesley, D. J. *J. Chem. Phys.* **1999**, *108*, 9737.
(39) Groot, R. D.; Warren, P. B. *J. Chem. Phys.* **1997**, *107*, 4423.
(40) Qian, H. J.; Lu, Z. Y.; Chen, L. J.; Li, Z. S.; Sun, C. C. *Macromolecules* **2005**, *38*, 1395.
(41) Li, X.; Deng, M.; Liu, Y.; Liang, H. *J. Phys. Chem. B* **2008**, *112*, 14762.
(42) Zhang, L.; Lin, J.; Lin, S. *Macromolecules* **2007**, *40*, 5582.
(43) Moffitt, M.; Vali, H.; Eisenberg, A. *Chem. Mater.* **1998**, *10*, 1021.
(44) Yusuf, H.; Kim, W.-G.; Lee, D. H.; Guo, Y.; Moffitt, M. G. *Langmuir* **2007**, *23*, 868.
(45) Jenekhe, S. A.; Chen, X. L. *Science* **1999**, *283*, 372.
(46) Lee, M.; Cho, B.-K.; Zin, W.-C. *Chem. Rev.* **2001**, *101*, 3869.
(47) Pinol, R.; Jia, L.; Gubellini, F.; Levy, D.; Albouy, P.-A.; Keller, P.; Cao, A.; Li, M.-H. *Macromolecules* **2007**, *40*, 5625.
(48) Ding, W.; Lin, S.; Lin, J.; Zhang, L. *J. Phys. Chem. B* **2008**, *112*, 776.
(49) Barmatov, E. B.; Pebalk, D. A.; Barmatova, M. V. *Langmuir* **2004**, *20*, 10868.
(50) Carlsen, A.; Lecommandoux, S. *Curr. Opin. Colloid Interface Sci.* **2009**, *14*, 329.
(51) Wong, M. S.; Cha, J. N.; Choi, K.-S.; Deming, T. J.; Stucky, G. D. *Nano Lett.* **2002**, *2*, 583.
(52) Iatrou, H.; Frielinghaus, H.; Hanski, S.; Ferderigos, N.; Ruokolainen, J.; Ikkala, O.; Richter, D.; Mays, J.; Hadjichristidis, N. *Biomacromolecules* **2007**, *8*, 3871.
(53) Wang, R.; Xu, N.; Du, F.-S.; Li, Z.-C. *Chem. Commun.* **2010**, *46*, 3902.
(54) Cai, C.; Wang, L.; Lin, J. *Chem. Commun.* **2011**, *47*, 11189.
(55) Blout, E.; Karlson, R. *J. Am. Chem. Soc.* **1956**, *78*, 941.
(56) Cai, C.; Zhang, L.; Lin, J.; Wang, L. *J. Phys. Chem. B* **2008**, *112*, 12666.
(57) Brust, M.; Walker, M.; Bethell, D.; Schiffrin, D.; Whyman, R. *J. Chem. Soc., Chem. Commun.* **1994**, 801.
(58) Brust, M.; Fink, J.; Bethella, D.; Schiffrina, D.; Kielyb, C. *J. Chem. Soc., Chem. Commun.* **1995**, 1655.
(59) Choo, H.; Cutler, E.; Shon, Y. *Langmuir* **2003**, *19*, 8555.
(60) Hong, B.; Qiu, F.; Zhang, H.; Yang, Y. *J. Chem. Phys.* **2010**, *132*, 244901.
(61) Jiang, T.; Wang, L.; Lin, S.; Lin, J.; Li, Y. *Langmuir* **2011**, *27*, 6440.
(62) Ortiz, V.; Nielsen, S. O.; Discher, D. E.; Klein, M. L.; Lipowsky, R.; Shillcock, J. *J. Phys. Chem. B* **2005**, *109*, 17708.
(63) Jeppesen, C.; Wong, J. Y.; Kuhl, T. L.; Israelachvili, J. N.; Mullah, N.; Zalipsky, S.; Marques, C. M. *Science* **2001**, *293*, 465.
(64) Koide, A.; Kishimura, A.; Osada, K.; Jang, W.-D.; Yamasaki, Y.; Kataoka, K. *J. Am. Chem. Soc.* **2006**, *128*, 5988.
(65) Wilcoxon, J. P.; Martin, J. E.; Provencio, P. *J. Chem. Phys.* **2001**, *115*, 998.
(66) Liz-Martin, L. *Langmuir* **2006**, *22*, 32.
(67) Yonezawa, T.; Kunitake, T. *Colloids Surf., A* **1999**, *149*, 193.
(68) Burchard, W.; Schmidt, M.; Stockmayer, W. *Macromolecules* **1980**, *13*, 1265.
(69) Wu, C.; Li, M.; Kwan, S.; Liu, G. *Macromolecules* **1998**, *31*, 7553.
(70) Chu, B. *Laser Light Scattering*, 2nd ed.; Academic Press: New York, 1991.
(71) Lin, S.; Numasawa, N.; Nose, T.; Lin, J. *Macromolecules* **2007**, *40*, 1684.
(72) Pryamitsyn, V.; Ganesan, V. *J. Chem. Phys.* **2004**, *120*, 5824.
(73) Song, W. D.; Tang, P.; Zhang, H. D.; Yang, Y. L.; Shi, A. C. *Macromolecules* **2009**, *42*, 6300.
(74) Flory, P. J. *Adv. Polym. Sci.* **1984**, *59*, 1.
(75) Kim, K. T.; Park, C.; Vandermeulen, G. W. M.; Rider, D. A.; Kim, C.; Winnik, M. A.; Manners, I. *Angew. Chem., Int. Ed.* **2005**, *44*, 7964.
(76) Checot, F.; Lecommandoux, S.; Klok, H.-A.; Gnanou, Y. *Eur. Phys. J. E* **2003**, *10*, 25.
(77) Bates, F. S.; Schulz., M. F.; Rosedale, J. H.; Almdal, K. *Macromolecules* **1992**, *25*, 5547.